

# PERFORMANCE DEGRADATION MODELLING OF ROTORCRAFT ENGINES OPERATING IN BROWNOUT CONDITIONS

Matthew Ellis<sup>1</sup>, Nicholas Bojdo<sup>2</sup>, Antonio Filippone<sup>3</sup>

School of Mechanical, Civil and Aerospace Engineering, University of Manchester (GBR)<sup>1,2,3</sup>

<sup>1</sup>matthew.ellis@manchester.ac.uk, <sup>2</sup>nicholas.bojdo@manchester.ac.uk, <sup>3</sup>A.Filippone@manchester.ac.uk

## ABSTRACT

Rotorcraft engines are subject to significant damage whilst operating in brownout conditions due to the ingestion of mineral particulates. The high pressure turbine is particularly at risk due to the deposition of molten particles on nozzle guide vanes and first stage rotor blades, causing a roughening of the surface and a reduction in efficiency. The rate of damage is non-linear; predicting the evolution of this damage has proven to be difficult given the wide range of contributory factors related to both engine and particulate. A first-order methodology is presented whereby component level losses in high pressure turbine nozzle guide vane efficiency can be translated via surface roughness changes into a performance loss of the whole engine. Component level computational fluid dynamics simulations are combined with an aerothermodynamic gas turbine model to evaluate reductions in engine performance during brownout operations for two rotorcraft using the same General Electric T700 engine. It is shown that the rate of engine degradation is proportional to the brownout concentration of the particular rotorcraft. Surface roughness changes alone are shown to be capable of producing up to a 1% reduction in the core mass flow rate and overall engine efficiency. This is demonstrated to occur after only 38 minutes of flight in brownout conditions for the Sikorsky HH-60 'Pave-Hawk' and 120 minutes for the Bell UH-1Y 'Venom'.

## 1. INTRODUCTION

### 1.1. Rotorcraft Brownout

Military rotorcraft have seen more frequent use in harsh environments in the last thirty years, through the first Gulf conflict and the more recent Iraq and Afghanistan campaigns. Exposure to these particulate laden environments has revealed operational concerns which previously were not considered to be major issues. At the forefront of these issues is 'brownout'. As shown in Figure 1, this is the production of dense clouds of mineral dust around the airframe during low altitude flight manoeuvres.



**Figure 1:** Production of a brownout cloud by the UH-60 'Black Hawk' at the Yuma Proving Ground<sup>[1]</sup>.

The production of brownout clouds poses many concerns to both rotorcraft and pilot. Firstly, the erosive nature of mineral dust causes abrasion and erosion of the external aircraft structure,

windshields and rotor blades. A more safety critical issue has been the ingestion of the generated dust cloud into the engines, where it can cause serious damage to critical engine components and ultimately induce engine failure in a multitude of ways<sup>[2]</sup>. The combination of these damage processes causes a reduction in sub-system efficiencies and therefore overall performance of the engine. Most critically, the accumulation of molten material in turbines and the erosion of compressor blades can reduce the mass flow rate through the engine. Ultimately this can reach a point at which the entire engine surge margin is consumed and flow reversal occurs<sup>[3]</sup>.

The main issue for the pilot arises due to the reduced visibility associated with brownout conditions and this can be exacerbated by erosion causing clouding of the windshields. This makes the already critical flight manoeuvres close to the ground more difficult and prolongs the duration of exposure of the engine to high particulate concentrations<sup>[4]</sup>. Brownout landings are considered the most difficult and dangerous manoeuvre in military aviation<sup>[1]</sup>. Indeed, several accidents resulting in both fatalities and platform loss have been attributed to the ingestion of particulate into engines during brownout. Most notably, the 2015 loss of a US Marines V-22 'Osprey' in Hawaii, where engine surge occurred after just 60 seconds in a dense dust cloud<sup>[5]</sup>.

The mechanism of production for brownout clouds

is the impingement of the rotor downwash jet against the ground. This induces the lofting of particles through a range of inertial transport mechanisms such as creep, saltation and suspension which are dependent upon the inertia of the particle and the local velocity field in the rotor downwash<sup>[1]</sup>. It should also be appreciated that the influence of each particle transport mechanism on the dust cloud produced will vary on a case-by-case basis depending upon the wake aerodynamics of the rotor under consideration; this is often termed the '*Brownout Signature*' of the platform, a characteristic which quantifies the concentration and structure of the dust cloud and therefore the quantity of dust that the rotorcraft's engines ingest.

Considerable previous work has been carried out to link the brownout signature of a rotorcraft with factors such as rotor configuration, blade design and fuselage shape<sup>[6]</sup>. It has been identified that it is difficult to attribute the intensity of a given platform's brownout signature and hence likelihood of sustaining damage to a single rotor design parameter. This is due to the inter-dependence of rotor design parameters such as blade chord, number and rotational speed upon the resulting rotor aerodynamics and hence the brownout cloud produced. Instead, it has been shown that the strength of the rotor wake has a significant effect upon the intensity of the cloud produced. Given that this is a function of the thrust, a general trend can be established between the disk loading of the rotor and the concentration of the brownout cloud. In general, as the disk loading and hence downwash velocity of the rotor is increased, the brownout severity increases<sup>[7]</sup>.

### 1.1.1. Brownout Mitigation

Currently the U.S. Military spends almost \$100 million per year on brownout related maintenance and platform losses<sup>[1]</sup>. This is mostly attributed to the deficiencies in predicting damage rates and therefore the operational lifetimes of engines operating in dusty environments. Indeed, it has been seen that engines removed after the same number of cycles show markedly different damage depending upon their location of operation and the individual missions undertaken. It is therefore understandable that a considerable research effort has been concentrated on the characterisation, formation and dispersal of brownout clouds and the identification of techniques and hardware which can mitigate its effect<sup>[8]</sup>.

In terms of preventing damage to engines, the most common protection from particulate ingestion for turboshaft engines is the use of

Engine Air-Particle Separator (EAPS) systems. These take the form of Vortex Tube Separators, Inlet Barrier Filters or Inertial Particle Separators. In a comparative analysis of these three technologies, it was shown that Inlet Barrier Filters are the most effective EAPS system with a particle removal efficiency of up to 98% for particles greater than 40 microns in diameter<sup>[9]</sup>. However, the separation efficiency drops rapidly for particles smaller than this. This has a marked effect upon engine damage as it is those particles with sizes 5 microns and above which are most likely to interact with and damage engine components. Therefore, we can expect that even with an EAPS system employed, there is still potential for an engine to become damaged.

### 1.2. GTE Damage & Performance Reduction

The damage seen in a turboshaft engine is a strong function of the engine, its architecture and operating state. Other important factors are the mineralogical and morphological properties of the particulate that is ingested and how these change during the passage of the particle through the engine.

Those particulates which have an inertia small enough such that they evade capture by the EAPS system can subsequently enter the core stages of a turboshaft engine and induce damage in a multitude of ways. Degradation of '*cold section*' components such as axial compressors occurs due to high velocity impact resulting in the physical removal of component material. This is generally concentrated on the pressure surface of blades causing pitting and cratering of aerofoil profiles, resulting in elevated losses due to increased surface roughness<sup>[10]</sup>. Additionally, the compressor is subject to abrasive wear, resulting in material removal at the rotor tips and casing wall as the particle moves between the two<sup>[2]</sup>. These effects combine to reduce the compressor pressure ratio and hence surge margin such that the working line begins to shift towards the surge line. Ultimately, these two will coincide and the engine will surge, resulting in a loss of power<sup>[11]</sup>. The compressor also has a marked effect upon the properties of the particulate, with possible pulverisation and milling occurring resulting in the size of particles reducing during their passage through the cold section.

Those particles which exit the compressor are then heated in the first '*hot section*', the combustor. Critically, if the temperatures are high enough in the combustor, a significant amount of this particulate may melt and deposit on the walls of the combustor annulus, potentially blocking fuel injectors, resulting in fuel starvation and ultimately engine flame out<sup>[2]</sup>.

Heated particles which exit the combustor next encounter the High Pressure Turbine (HPT) NGVs. This is the location of arguably the most critical damage mechanism, where molten particulate from the combustor interacts with these vanes and deposits. This acts to reduce turbine performance in two ways; physical area blockage and increased skin friction. As shown in Figure 2, the accumulation of these deposits reduces the throat area in the nozzles and therefore the engine mass flow rate at a given engine pressure ratio. The structures of the deposits are themselves inherently rough, and the extra skin friction losses this introduces result in an additional reduction in the mass flow. The combined effect of these two mechanisms is to decrease the turbine flow capacity and efficiency. This reduction in turbine mass flow dictates the compressor mass flow must also decrease. This acts in conjunction with compressor degradation to further reduce the surge margin of the engine<sup>[11]</sup>.



**Figure 2:** HPT NGV damage from molten particulate accumulation<sup>[2]</sup>.

The accumulation of molten deposits in turbine stages has secondary damage implications. The first of these is to block impingement cooling channels and film cooling holes. This inhibits heat transfer from the blade metal into the cooling fluid which is critical in order to keep the blade surface in its safe operating range. As internal deposits build up, the vane temperature and commensurate thermal stresses increase, resulting in high temperature creep deformation and potentially blade fracture. However, external surface deposits act to insulate the vane, protecting it from the thermal stresses introduced by internal deposition. As a result, chemical reaction of the molten particulate with the surface to which it is bonded is arguably more of a risk. The extent of this hot corrosion and sulphidation is a function of the mineral composition of the dust in its molten state<sup>[12]</sup>. Hot corrosion and sulphidation of the alloy has in some cases been seen to burn holes in vanes and cause cracking at the blade root. The extent of this corrosion is currently believed to be related to the quantity of gypsum in the ingested particulate<sup>[13]</sup>.

## 2. LITERATURE REVIEW

### 2.1. Erosion Surface Roughness

In each of the erosion, abrasion and deposition engine damage mechanisms already described, the common consequence is the deterioration of component surface finishes<sup>[14]</sup>. The result of this increase in surface roughness is additional aerodynamic losses and engine performance degradation.

There has been a significant amount of previous work carried out to characterise the performance losses seen by the whole engine due to degradation of turbine component surfaces. The majority of this work has centred on the erosion of low pressure turbine (LPT) stages and the application of surface treatments such as thermal barrier coatings that increase roughness. Boynton et al.<sup>[15]</sup> showed that reducing the turbine roughness by two orders of magnitude resulted in a 2.5% change in efficiency for an axial flow turbine stator vane. The choice of component material or surface treatments can also have a significant effect upon the losses seen in the turbine cascade. Indeed, Boyle and Senyitko<sup>[16]</sup> found that while the use of a Zirconium thermal barrier coating (TBC) increased the surface roughness, for certain flow Reynolds numbers a reduction in profile losses was experienced compared to a smooth vane. This was attributed to the rough surface delaying the boundary layer transition. For all other Reynolds numbers the additional profile losses increased due to roughness-induced transition and increased momentum losses in the turbulent boundary layer from 40% up to a maximum of 60%. Matsuda et al.<sup>[17]</sup> carried out testing on a full-scale HPT cascade observing the profile and end-wall pressure losses for a range of surface finishes. Again, it was observed that an optimum roughness occurs for low Reynolds numbers at which the total pressure loss reduces slightly before increasing again. Hummel et al.<sup>[18]</sup> carried out a similar study using a slightly reduced surface roughness on a similar LPT and found the additional profile loss to be between 20% and 50% of the baseline loss. Crucially, it was observed that the additional pressure loss increased proportionally with the flow Reynolds number with no region of ideal roughness present.

One of the most comprehensive studies carried out previously was that of Kellersman et al.<sup>[19]</sup> A coupled CFD-Engine Performance analysis of a five stage LPT cascade was carried out, using surface roughness values for each stage obtained from used engine components. The equivalent roughness values used in this study were relatively modest (0-10 microns) and indicative of

erosive damage. The CFD analysis showed an increase in surface averaged skin friction coefficient with increasing roughness due to premature boundary layer transition. The total efficiency loss for the LPT was calculated to be 0.16%. Using a gas path analysis, it was subsequently shown that this reduction in LPT efficiency results in a 0.06% increase in fuel flow rate and a 1.2K rise in exhaust gas temperature (EGT). These performance changes were determined to be equivalent to a 4% change in the EGT and hence engine surge margin.

## 2.2. Accretion Surface Roughness

By contrast, the accumulation of molten material in the HPT is rarely described in terms of changes in surface roughness despite the accretion process resulting in significantly higher levels of roughness than the erosion we tend to see in the LPT. Therefore the performance losses presented in the work already discussed are analogous only to the surfaces of mildly degraded NGVs.

Jensen et al.<sup>[20]</sup> were the first to quantify the accumulation of particulate using surface roughness metrics. Using an accelerated deposition rig to replicate the conditions at the HPT NGV stage of a gas turbine engine, the evolution of molten deposits on coated, rectangular metal coupons was investigated for a range of inclination angles (representative of the stagger angle for a turbine vane). The thickness of deposits formed was mapped using a diamond-tipped profilometer at a series of time intervals and converted into an equivalent surface roughness, thus quantifying the deposit evolution.

Wammack et al.<sup>[21]</sup> extended this to include the evaluation of a range of surface treatments, using the same facility and processing methods to determine the surface topologies of a Nickel-Cobalt superalloy and two different TBC coupons inclined at 45 degrees to the flow and subjected to the same particulate concentration for the same time period. The main observation of this work was that the peak surface roughness obtained for deposition is almost an order of magnitude higher than those associated with erosion damage (150 microns being the highest in this study). It was seen that the surface roughness grows rapidly at first, followed by a steady period in which peaks and troughs become filled and finally another rapid roughness increase. They saw that whilst the TBC coated surfaces have a higher reference roughness, they experienced significantly lower peak roughness for a given particle exposure time.

Generally, the surface roughness changes associated with abrasion and erosion are much smaller than those which characterise deposition.

Consequently, we can reasonably expect the HPT efficiency losses due to deposition induced roughness to be much higher than those already discussed for LPT pressure losses. It would therefore be useful to find a relationship between the quantity of particulate that accumulates on NGVs, and the surface roughness change associated with this. By linking the roughness change to the efficiency loss of the turbine stage and sub-system, it then becomes possible to begin to analyse the effect this degradation has on the performance of the whole engine.

## 3. THEORY & METHODOLOGY

In the current work, we restrict our analysis to 'accretion-induced' surface roughness on the nozzle guide vanes, due to the relative abundance of experimental data in the literature. However, this method could also be applied to determine performance losses due to surface roughness changes of other engine components.

### 3.1. CFD Modelling

A two-dimensional CFD model has been developed using the commercial solver STARCCM+. The geometry used is the NGV stage of the General Electric Energy Efficient Engine (GE-E<sup>3</sup>). Ideally, the HPT NGV geometry of the T-700 engine would be used, however this is not available in the open literature. The flow was solved using a Second Order Upwind discretisation of the Reynolds Averaged Navier-Stokes equations. Turbulent velocity fluctuations in the near wall boundary region were handled through the use of the Menter  $k-\omega$  SST model and its rough wall functions. This allows the component performance loss for the NGV stage under various deposition induced roughness conditions to be assessed. The determined flow characteristics are used to calculate the stage performance losses for each surface roughness.

#### 3.1.1. Geometry & Meshing

Two vanes of the NGV stage have been modelled with the use of periodic boundary conditions to reduce the size of the computational domain. The inflow is modelled as a velocity inlet whilst exit conditions are handled using a pressure outlet. The outflow is spaced 1.5 vane chords aft of the trailing edge of the NGV in order to allow the wake to fully develop, preventing reversed flow on the outlet boundary and hence numerical instability.

Meshing of the computational domain was carried out using the inbuilt grid generation functions within the STARCCM+ solver. The mesh was unstructured and used tetrahedral elements and a 40 layer prism mesh was employed at the vane surface. This was applied to ensure that the

turbulent boundary layer was fully resolved giving a dimensionless wall distance,  $y^+$ , of less than unity around the whole vane. The resulting grid independent mesh incorporated 155,447 cells and is shown in Figure 3.

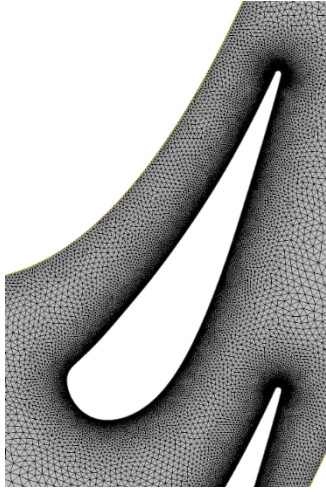


**Figure 3:** The computational domain used for CFD calculations.

### 3.2. Surface Roughness

The introduction of surface roughness to any fluid flow problem can be expected to increase losses due to friction. Whilst some surfaces are often described to be '*dynamically smooth*' these surfaces still have a residual level of roughness. However, the associated friction losses are negligible. It would be useful to be able to relate the pressure loss to the amount of particulate ingested via the roughness. This can then be used to assess the efficiency loss that results at component and the overall engine scales.

#### 3.2.1. Surface Roughness Measurement

The measurement of surface roughness for gas turbine engine blading is usually carried out using a contact-stylus system in which the stylus follows the surface features of a part. The output of this device is a height profile in a particular direction, which if carried out in two orthogonal directions can be used to develop a three-dimensional profile of the surface topology.

Despite this level of detail being available for a given surface, its use is fairly limited, as most surface roughness modelling is carried out using a single roughness value. Multiple surface roughness metrics exist, with the most commonly reported of these being the centreline average roughness height,  $Ra$ , defined as:

$$(1) \quad Ra = \frac{1}{IJ} \sum_{i=0}^{I-1} \sum_{j=0}^{J-1} |z_{i,j}|$$

Where  $I$  and  $J$  are the number of surface data

points in the  $x$  and  $y$  directions respectively and  $z_{i,j}$  is the height of an individual surface element relative to a specified datum line<sup>[21]</sup>. This effectively represents the average surface heights at a number of discrete  $x, y$  points on the surface.

The Root Mean Square (RMS) roughness,  $Rq$  is an extension of the centreline average, defined as the root mean square sum of the measured height at each discrete location ( $z_{i,j}$ ):

$$(2) \quad Rq = \sqrt{\frac{1}{IJ} \sum_{i=0}^{I-1} \sum_{j=0}^{J-1} |z_{i,j}|^2}$$

In general, either the centreline averaged roughness or the RMS roughness are reported as they account for spatial variations of roughness on a surface unlike the maximum peak to valley roughness.

#### 3.2.2. Incorporation into CFD

As has been identified, the pressure surface of vanes are more likely to accumulate molten particulates and therefore have elevated surface roughness. However, the suction surface rarely sees particulate impacts and it therefore maintains a relatively constant level of roughness and is treated as smooth.

Whilst it is possible to use experimental techniques to establish a three dimensional surface topography, implementation of this into a CFD code would require a complex geometry to account for all peaks and troughs on the surface. These small scale geometry features result in the need for much finer meshes and drastically elevated computing time for a given case. Instead, commercial CFD codes such as STARCCM+ require the specification of a single, spatially uniform roughness parameter; the 'equivalent sandgrain roughness',  $k_s$ . This is defined as the roughness feature that has the 'equivalent' effect on skin friction losses as a uniform layer of sandgrains with diameter  $k_s$ .

Measuring an equivalent sand grain roughness is not possible and therefore it is usually correlated to other roughness parameters, most commonly to the centreline averaged roughness. A comprehensive review of these correlations was carried out by Bons<sup>[22]</sup> who identified wide variability depending upon the type of the initial surface. Within this, multiple correlations exist for turbine blade surfaces and the author acknowledged the difficulty in choosing an appropriate relationship.

In this work, the correlation of Bogard et al.<sup>[23]</sup> has been implemented as this was identified by Bons<sup>[22]</sup> to be the most suitable for bare metal turbine

blade surfaces [22]. It is given by Equation 3:

$$(3) \quad k_s \approx 4R_a$$

The centreline averaged surface roughness measurements made by Wammack et al. [21] after four deposition 'burns' on a Nickel-Cobalt superalloy surface can each be converted to an equivalent sandgrain roughness using the correlation presented in Equation 3. Table 1 gives a quantification of the surface roughness evolution that can be implemented into the CFD model on the pressure surface of the vane.

Surface Type	Burn #	$R_a$ [ $\mu\text{m}$ ]	$k_s$ [ $\mu\text{m}$ ]
Nickel-Cobalt Superalloy	-	0	0
	1	2	8
	2	13	52
	3	18	72
	4	38	152

**Table 1:** Surface Roughness Conversion for the Nickel-Cobalt superalloy deposition measurements from [21].

The effects of surface roughness in STARCCM+ are incorporated using a modified version of the log-law for the wall. A roughness function,  $f$  is used to modify the standard log-law coefficient,  $E$  in Reichardt's blended wall law:

$$(4) \quad f = \begin{cases} 1 & R^+ \leq R^+_{Smooth} \\ [0.253R^+]^a & R^+_{Smooth} < R^+ < R^+_{Rough} \\ 0.253R^+ & R^+_{Rough} \leq R^+ \end{cases}$$

Where the exponent,  $a$  is given by:

$$(5) \quad a = \sin \left[ \frac{\pi}{2} \frac{\log(R^+/R^+_{Smooth})}{\log(R^+_{Rough}/R^+_{Smooth})} \right]$$

The form of Equation 4 depends upon the value of  $R^+$  compared to two critical values;  $R^+_{Rough}$  and  $R^+_{Smooth}$ . The roughness parameter  $R^+$  is given by:

$$(6) \quad R^+ = \frac{k_s u^*}{\nu}$$

The reference velocity,  $u^*$  is related to the wall shear stress and  $\nu$  is the kinematic viscosity of the fluid.

### 3.3. Particulate Characterisation

As we have already identified, the damage effects depend upon the inertial, rheological and morphological properties of the dust [12, 24]. These are known to be functions of the size distribution and the mineralogy of the dust. Two different types of particulate have been considered in this work. The first of these dusts is that used in the experimental deposition tests of both Jensen et al.

and Wammack et al. at Ohio State University (OSU) [21, 22]. It was deposits of this dust from which the surface roughness quantities in Table 1 were derived. The second particulate is that of the Yuma Proving Ground (YPG) in Arizona, USA where the Sandblaster 2 tests were undertaken to characterise the brownout signatures of different rotorcraft [7]. It is airborne distributions of this dust from which the brownout concentrations in Table 2 were derived. It is important to ensure that the particulates have similar size distributions and mineralogical compositions and therefore comparable inertial and morphological behaviour. If this is true then we are subsequently able to combine the results obtained for these two different particulate sources, and link roughness damage to brownout concentration

#### 3.3.1. Particle Size

The size of a particle has been identified as a critical factor in determining its likelihood of hitting a surface, depositing and hence causing a change in surface roughness. For any given sample of particle ingested by an engine, we can expect to see a range of particle sizes. The comparison of the cumulative size distributions for the OSU and YPG dusts is shown in Figure 4.

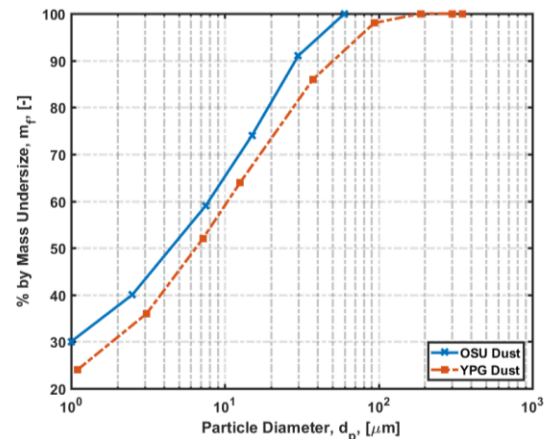


**Figure 4:** Cumulative Size Distributions for the OSU and YPG dusts.

In general, we see that the size distributions are similar but the OSU dust is skewed towards smaller diameters compared to YPG. This would be expected given that OSU is a manufactured dust designed specifically to have diameters between 0-80 microns whilst the YPG dust is 'ambient' and therefore naturally contains a proportion of particles with diameters greater than 100 microns. We would therefore expect that the deposition results of the OSU dust are over-predictions compared to that of the YPG dust for an equal mass of ingested particulate.

#### 3.3.2. Mineralogical Composition

Similarly, the mineralogical compositions of the

two dusts have been analysed in Figure 5. This shows us that the only significant difference between the OSU and YPG dusts is the increased proportions of Calcite (CaO) and Hematite (Fe<sub>2</sub>O<sub>3</sub>) at the expense of a reduction in Quartz (SiO<sub>2</sub>) content in the YPG dust. We can make a reasonable assumption that the rheological and morphological properties of the dusts are comparable and hence will form similar deposit structures.

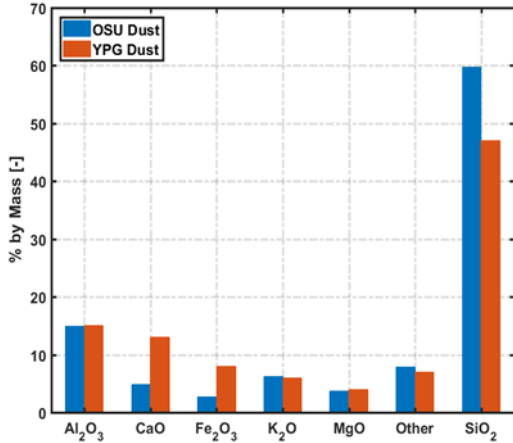


**Figure 5:** Mineralogical Compositions of the OSU and YPG dusts.

### 3.4. Particulate Dosage

Being able to determine the amount of particulate ingested by an engine during a particulate encounter such as brownout is critical in being able to make assessments of the amount of damage that an engine can tolerate. The most commonly used method in the past has been to use a dust concentration and a given exposure time in conjunction with the engine mass flow rate to determine the total mass of dust that is ingested. However this is contingent on the bulk density of the particulate being known. Clarkson et al.<sup>[3]</sup>, have since suggested that the use of a 'dosage' may be a more appropriate means of categorising particulate encounter events. This is suggested due to the fact that events can occur at a wide range of concentrations and over various durations. In the case of brownout this depends upon the rotorcraft and its brownout signature and also the mission being operated. The 'dose' is therefore defined as the product of the particulate cloud concentration, C and the duration of the encounter,  $t_b$ .

$$(7) \quad \delta = \sigma_p t_b$$

### 3.5. Engine Performance Modelling

As in-flight engine performance data becomes more comprehensive and readily available, the ability to understand how this relates to an engines health becomes useful for operators. In

order to do this, relationships between the amount of particulate ingested and changes in engine performance parameters are required. The use of engine performance modelling codes allows these damage induced variations to be assessed.

#### 3.5.1. The T-700 Engine

The General Electric T700 turboshaft engine is a widely used powerplant in military rotorcraft operations. The Sikorsky, HH-60 'Pave Hawk' and Bell UH-1Y 'Venom' platforms both use this powerplant. The T700 engine is a two-spool design comprising a high pressure gas-generator turbine driving a high pressure radial flow compressor and a low pressure power turbine driving a low pressure axial compressor.

#### 3.5.2. High Pressure Turbine Performance

Each module of the engine such as the HPT is split into a series of stages, the performance of which can be analysed independently using stage design parameters. The performance of an axial turbine stage can be described by a series of non-dimensional coefficients.

The flow coefficient is the ratio of the axial flow velocity,  $V_x$ , through the stage to the rotational speed of the rotor,  $U$ :

$$(8) \quad \phi = \frac{V_x}{U}$$

The stage loading is defined as the ratio of the stagnation enthalpy drop across the stage to the tangential speed of the rotor:

$$(9) \quad \psi = \frac{2 c_p (T_{01} - T_{03})}{U^2}$$

Where  $c_p$  is the specific heat capacity of the working fluid and  $T_{01}$  and  $T_{03}$  are the stagnation temperatures at the stage inlet and exit respectively.

The stage reaction is the ratio of the expansion and hence enthalpy drop in the rotor compared to that across the whole stage. This can be expressed in terms of the static temperature drop across the rotor compared to the whole stage.

$$(10) \quad \Lambda = \frac{T_2 - T_3}{T_1 - T_3}$$

The flow described by these coefficients is subject to losses, resulting in a drop of the overall stage efficiency. These can be split broadly into the losses in the nozzle and rotor respectively. In this work, it is idealised that degradation in the nozzle and the losses associated with this do not cause further losses in the rotor or latter stages of the HPT. Therefore the stage efficiency loss is equal to the high pressure turbine efficiency loss.

The nozzle loss coefficient describes the additional loss of stagnation pressure that occurs due to skin friction in the nozzles. It is given by Equation 11:

$$(11) \quad \lambda_N = \frac{T_2 - T_2'}{C_2^2 / 2c_p}$$

Where  $T_2$  is the static temperature at the nozzle exit,  $T_2'$  the ideal isentropic nozzle temperature and  $C_2$  the absolute velocity at the nozzle exit.

We can expect that as the surface finish of the nozzle blades degrades, the loss coefficients will increase, resulting in a reduction in the overall stage efficiency. Cohen et al. [25] showed that the nozzle loss coefficient can be used to describe the overall stage efficiency, assuming no losses occur in the rotor as:

$$(12) \quad \eta_s = \frac{1}{1 + \left[ \left( \frac{T_3}{T_2} \right) \lambda_N \left( \frac{C_2^2}{2c_p} \right) \right] / (T_{01} - T_{03})}$$

### 3.5.3. Gas Turbine Simulation Program (GSP)

An aero-thermodynamic model of the T700 engine has been implemented using the Gas Turbine Simulation Program (GSP) developed by NLR [26]. GSP requires the specification of engine performance at a given design point. The off-design performance of the engine around this point is then determined by interpolation of a set of component maps [26]. Deteriorated performance of the engine can be simulated by providing efficiency changes for each sub-system. In this case, the HPT. The model developed is based upon the design point data available from previous numerical models of this engine [27].

### 3.6. Methodology

The coupled CFD-Engine-Performance methodology outlined in Figure 6 has been developed and implemented to assess the engine performance penalties associated with HPT NGV damage for turboshaft engines operating in brownout conditions.

The deposition evolution on nozzle guide vanes is expressed as a series of discrete surface roughness values. The CFD model developed in the commercial code STARCCM+ is then used to evaluate the NGV stage component loss. Gas turbine design theory is subsequently applied to translate this into an efficiency loss for the overall HPT stage. This is then incorporated into a zero-dimension engine performance model of the General Electric (GE) T700 engine. The model is built within GSP and allows the performance loss of the whole engine to be assessed. Through the use of known experimentation and brownout flight testing, reductions in engine performance can be

correlated to brownout flight resulting in various particle dosages. This process is carried out for two rotorcraft, the Bell UH-1Y 'Venom' and the Sikorsky HH-60 'Pave Hawk' whose brownout signatures were characterised in the Sandblaster 2 testing campaign and which both use the T700 engine.

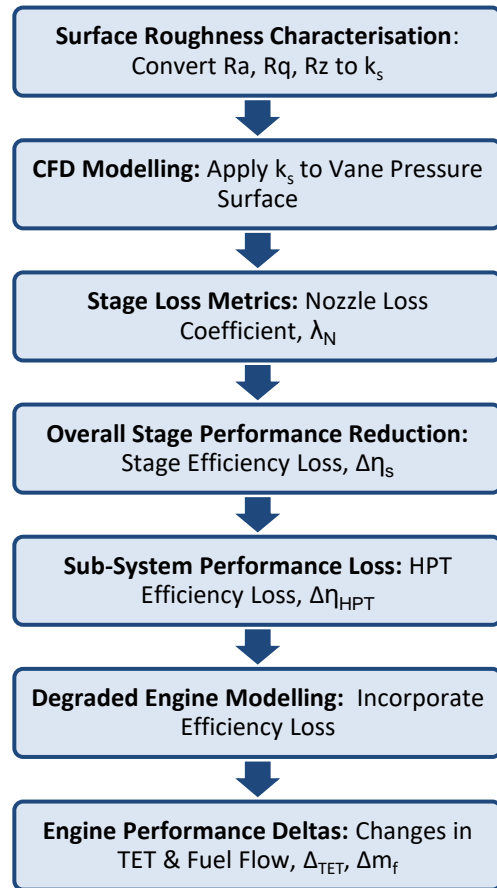


**Figure 6:** Workflow to couple CFD modelling of surface roughness with overall engine performance modelling via stage performance theory.

## 4. RESULTS & DISCUSSION

### 4.1. Turbine Stage Performance Degradation

The surface roughness properties shown in Table 1 were assigned to the pressure surface of the NGV in the CFD model. The pressure and velocity fields around the vane were then solved and the total pressure drop across the NGV stage was calculated for each surface roughness. When it became clear that a trend between the total pressure loss and the surface roughness was apparent, a series of additional, intermediate roughness values to those in Table 1 were also assessed. Each roughness value constitutes a state of degradation of the NGV. The results of this are plotted in Figure 7:

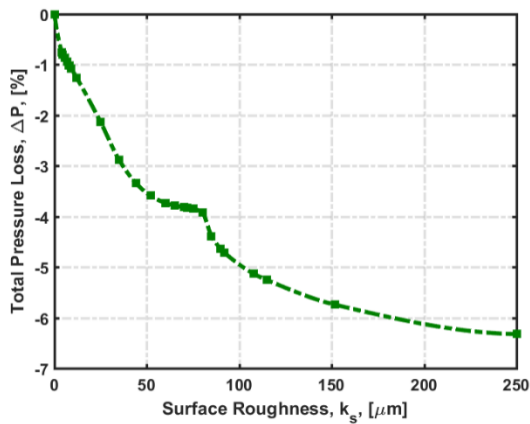


**Figure 7:** Relationship between NGV Surface Finish and Total Pressure Loss

We can see that as the amount of deposited particulate and hence the surface roughness increases, there is a commensurate increase in the pressure drop across the stage. This increases the viscous losses in the boundary layer around the NGV as the rough wall results in laminar-turbulent boundary layer transition earlier along the vane chord.

The effect that deposition induced surface roughness has on HPT performance can be assessed from the flow coefficient and stage loading under each degradation state. This can be represented by plotting the variation of these two parameters with increasing roughness on the turbine stage design ‘Smith Chart’ as shown in Figure 8.

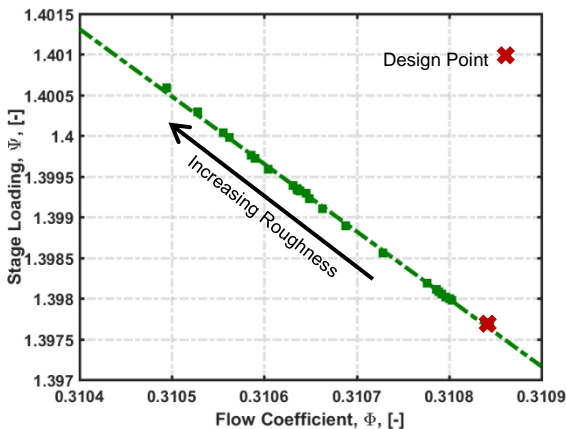


**Figure 8:** A Smith Chart showing how the design point of the 1<sup>st</sup> HPT stage moves with increasing roughness and hence deposition.

We see that a change in surface roughness from 0 $\mu$ m to 250 $\mu$ m results in a 0.32% increase in the flow coefficient and a 0.16% reduction in the stage loading. This increase in flow coefficient occurs due to the reduction in the nozzle exit flow velocity and therefore kinetic energy with increasing surface roughness. This work has not considered the effect deposition has on the surface geometry

change. Therefore we can expect this reduction in kinetic energy and therefore absolute velocity to be due to roughness only, not due to any changes in the outlet flow angle. The elevated stage loading arises as a result of the increase in the temperature drop ( $T_{01} - T_{03}$ ) across the stage as the surface becomes rougher. This is due to the dissipation of the kinetic energy discussed above as additional thermal energy. The result of this is in an increase in the total temperature at NGV outlet and therefore an increase in  $T_{01}$  at NGV inlet in order to maintain thermodynamic equilibrium.

Figure 8 shows us that the HPT performance begins to shift away from its design point due to increases in roughness. However, it does not give us any measure of the extent of the stage efficiency reduction. Making the assumption that the only efficiency reduction due to roughness occurs in the first stage of the HPT and that no additional downstream losses are caused by this, we can use Equation 12 to define the stage efficiency for each roughness case. Assuming this is equal to the efficiency reduction of the whole HPT, we can relate this to the deposition roughness in Figure 9.

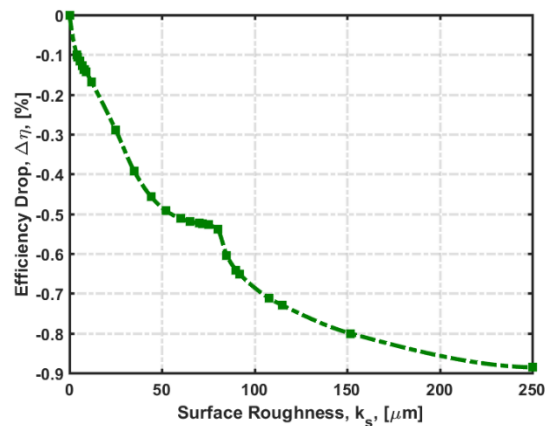


**Figure 9:** Efficiency drop of the HPT sub-system with surface roughness.

The efficiency loss of the first HPT stage follows the same trend as the total pressure loss with surface roughness. We would expect this as the two are intrinsically related through Equation 12. We can clearly see that the performance loss of the NGV and its stage is non-linear. This reflects the observations of Clarkson and Simpson<sup>[11]</sup> that the rate at which material accumulates on NGV surfaces is non-linear and therefore so is the performance loss.

The asymptotic discontinuity that is evident in both Figure 7 and Figure 9 arises due to the mathematical form of the roughness equation. The blended wall law used to model the velocity in the turbulent boundary layer takes a logarithmic

form. This is then modified using the discontinuous function in Equation 4 to adapt the log-law coefficient. When we combine the different modifications made to the Roughness Parameter,  $R^+$  for each range with the blended wall law, we see different asymptotic limits in each range.

#### 4.2. Engine Performance Degradation

The HPT sub-system efficiency reduction due to deterioration corresponding to each surface roughness in Table 1 was incorporated into the zero-dimension engine performance model. For each change in HPT efficiency the performance parameters required to maintain the engine design point free power turbine shaft power were calculated. These were then compared to the undeteriorated design point performance of the engine to get the percentage change in performance parameters. This is demonstrated in Figure 10 which shows how the design point performance parameters of the engine shift as the surface roughness degrades.

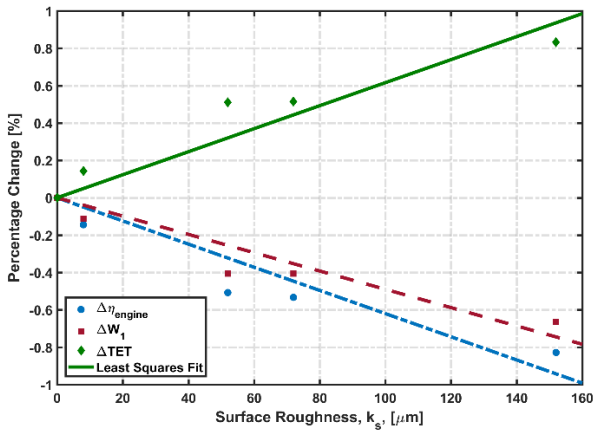


**Figure 10:** Variation in engine performance parameters with increasing surface roughness due to deposition in the HPT NGV.

From Figure 10 it is clear that the shifting of the first stage of the HPT away from its design point also causes the performance of the whole engine to deviate from its design point. Increases in the specific fuel consumption and the HPT exit temperature are observed whilst reductions in the overall engine cycle efficiency and core mass flow rate are seen. The performance of the engine is shown to vary linearly over the roughness range 0-160  $\mu\text{m}$  although above this requires additional future investigation as it may reveal the non-linear trends predicted by Clarkson and Simpson [11]. It should also be noted that the reduction in core mass flow in Figure 10 accounts for the reduction in mass flow due to surface roughness induced reductions in axial flow velocity. It does not account for core mass flow reductions as a consequence of throat area reduction due to molten particle deposition. It would be expected

that the magnitude of the changes in these parameters would be considerably greater if the effects of area blockage could also be incorporated into the model in the future.

#### 4.3. Relating Roughness to Dosage

Whilst surface roughness has allowed us to draw a link between the degradation of NGV's at a component level and the deterioration of the whole engine during brownout, its applicability is limited, due to the inability to monitor surface roughness in flight. In order to be able to use modelling approaches such as that demonstrated in Sections 3.1 and 3.2, operators require the reduction in engine performance to be related to another operational parameter they can easily predict or measure such as the flight duration.

The particulate 'dosage' combines duration and concentration into a single parameter, allowing brownout events at different concentrations and durations to be compared. Brownout testing during the Sandblaster campaign characterised the dust cloud concentrations of YPG dust for both the HH-60 and UH1-Y rotorcraft along with features of their rotor downwash. This is summarised in Table 2 below:

Rotorcraft	Rotor Tip Concentration [mg/m <sup>3</sup> ]	Disk Loading [N/m <sup>2</sup> ]
UH-1Y	310	239
HH-60	1160	383

**Table 2:** Summary of brownout characteristics for the UH-1Y and HH-60 rotorcraft [7].

The results already presented in Table 1 can be viewed as an evolution of the surface roughness with increasing exposure times to the OSU particulate. Each 'burn' carried out was for a relatively low particulate concentration over a long duration compared to those generally seen during brownout. From these durations and concentrations, it is possible to derive a dosage for each surface roughness through the use of Equation 7. This is demonstrated in Table 3:

Burn #	t <sub>burn</sub> [min]	C [mg/m <sup>3</sup> ]	k <sub>s</sub> [μm]	δ [g.s/m <sup>3</sup> ]
1	120	68.4	8	493
2	240	68.4	52	985
3	360	68.4	72	1478
4	480	68.4	152	1971

**Table 3:** Conversion of the experimental data from [21] to particulate 'dosages'

Establishing a dosage for each surface roughness allows us to relate the dosage via this surface

roughness to the reductions in engine performance parameters presented in Figure 10. The deviation of engine performance parameters away from the engine design point can therefore be represented as functions of the particulate dosage rather than the surface roughness:

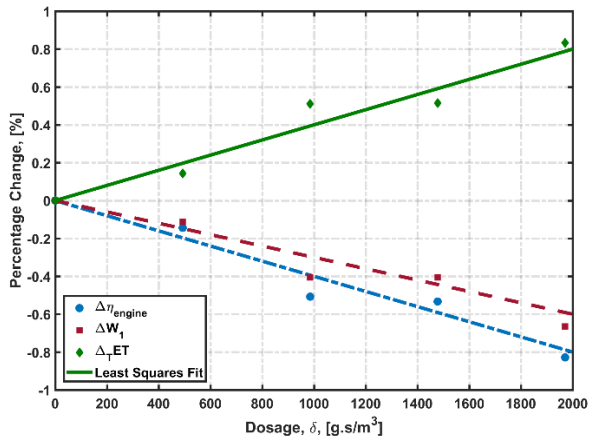


**Figure 11:** Variation in engine performance parameters with increasing surface roughness due to deposition in the HPT NGV.

As with surface roughness, these performance parameters can be related linearly to the dosage. The magnitude of the gradients of these curves represent the rate at which a particular performance metric degrades with increasing particulate dosage. We can therefore see that the reduction in overall engine efficiency and increase in the turbine exit temperature are the major operational concerns due to HPT damage. These would therefore be suitable metrics for operators to use from the point of view of predicting engine health in brownout situations.

The main benefit of plotting these performance reductions as a function of the dosage is that they allow a link to be drawn between the amount of particulate ingested, the surface roughness change and the rate of degradation. This would be applicable to any platform using the T700 engine were improvements to the model possible such as using the exact NGV geometry for the T700 engine. The results shown in Figure 11 show us the general trends of engine performance reduction with increasing dosage, applicable for any rotorcraft equipped with the T700 engine. However, for an operator it is likely to be more informative to observe how these vary with flight duration. The motivation to use this particular metric is mainly due to the time-critical nature of engine damage in brownout clouds.

It is possible to express the results presented in Table 3 as high concentration, short duration events more analogous to flight in brownout conditions. This allows us to relate engine performance reductions to the time spent in a

brownout cloud. We can expect that these durations will be dissimilar for the HH-60 and UH-1Y due to their vastly different dust cloud concentrations. Using the rotor tip brownout concentrations outlined in Table 2 we can apply the dosage principle to determine flight durations for the UH-1Y and HH-60 rotorcraft which would constitute these dosages.

Rotorcraft	$k_s$ [ $\mu\text{m}$ ]	$\delta$ [g.s/m <sup>3</sup> ]	C [g/m <sup>3</sup> ]	$\Delta t$ [min]
UH-1Y	8	493	0.31	26
	52	985	0.31	53
	72	1478	0.31	80
	152	1971	0.31	106
HH-60	8	493	1.16	7
	52	985	1.16	14
	72	1478	1.16	21
	152	1971	1.16	28

**Table 4:** Determination of the brownout flight durations required by the UH-1Y and HH-60 rotorcraft to achieve the dosages in Table 3

We now have a method by which we can relate the roughness of the deposition surface to the duration of flight in a given brownout concentration. This allows us to relate the changes in engine performance parameters shown in Figure 11 to a given flight duration in brownout for the HH-10 and UH-1Y platforms.

As was previously identified, the loading of a stage increases as its performance deteriorates. The result of this is that the temperature at the turbine exit is higher than its design point value. A by-product of this is that the temperatures throughout the engine increase in order to maintain thermodynamic equilibrium. The effect of degradation on TET is shown in Figure 12 for the HH-60 and UH-1Y. The rates at which the turbine exit temperature and therefore engine degradation evolve are represented by the gradients of the two lines in Figure 12. As we would expect, given its higher brownout concentration, a HH-60 equipped with the T700 powerplant is subject to a degradation rate from engine design point that is 3.75 times faster when compared to the UH-1Y with the same engine. This is due to the brownout concentration of the HH-60 being higher than that of the UH-1Y by the same factor of 3.75. Therefore, the HH-60 receives the dosage required to achieve each percentage performance reduction more rapidly than the UH-1Y.

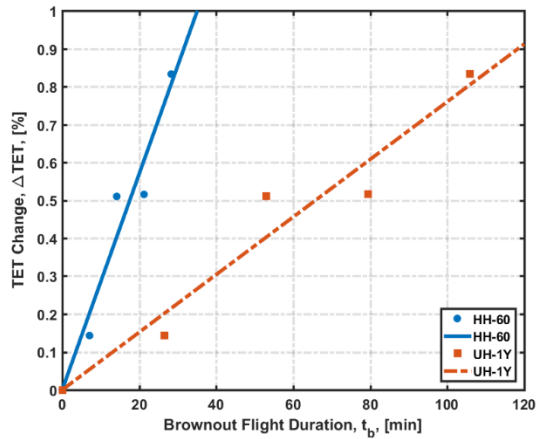


**Figure 12:** Increase in Turbine Exit Temperature with flight duration for the UH-1Y and HH-60 rotorcraft

The critical parameter in determining how the working line of the compressor shifts towards the surge line and hence the reduction in compressor surge margin is the change in core mass flow rate. This can also be represented as a function of the flight time in brownout conditions as shown in Figure 13. It should be noted that the reductions in mass flow rate presented here are those due to changes in surface roughness only. Therefore, this only accounts for mass flow reductions due to increased skin friction and not for the additional mass flow reductions due to area blockage. If we were to account for these area related losses then we would expect the total loss in core mass flow for both platforms to be significantly higher than those presented in Figure 12.

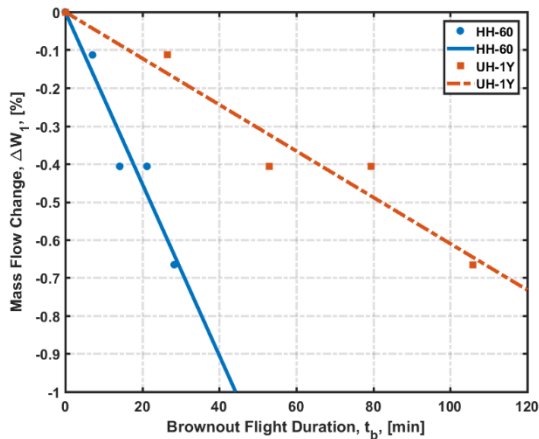


**Figure 13:** Reduction in core mass flow with flight duration for the UH-1Y and HH-60 rotorcraft

Finally, Figure 14 shows how the reduction in mass flow and increase in TET combine to reduce the overall efficiency of the T700 engine when fitted to the HH-60 and UH-1Y. Both rotorcraft have the potential to experience up to a 1% reduction in their efficiency. Comparing this to previously reported reductions in the LPT

efficiency of 0.16%<sup>[19]</sup> we can see that accounting only for roughness changes due to deposition we obtain an efficiency loss of the overall engine which is five-fold greater than that previously modelled for a degraded LPT. It should be remembered that the performance reductions estimated here account for roughness damage in the NGV only. They do not account for additional efficiency reductions that can occur due to blockage effects or losses in downstream components. In reality, we would therefore expect the overall efficiency change to be greater due to these additional degradation effects.

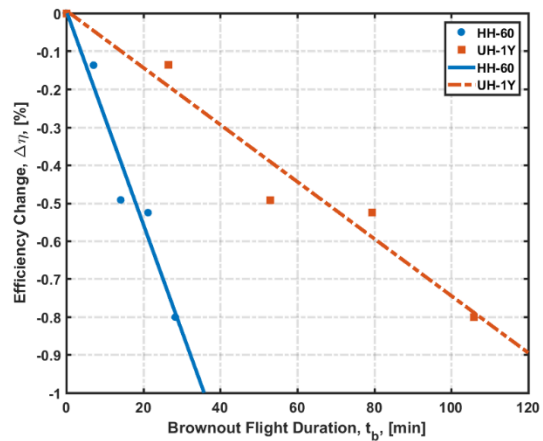


**Figure 14:** Duration of flight in Brownout versus Engine Efficiency loss for the HH-60 and UH-1Y Rotorcraft.

## 5. CONCLUSIONS

A methodology has been demonstrated which predicts the performance deterioration of rotorcraft using the T700 engine during operation in brownout. Past experimentation of particle deposition has been used to derive brownout durations for the HH-60 and UH-1Y rotorcraft. Using the dosage principle, low concentration, long duration results are converted into more appropriate short duration exposures based upon known brownout concentrations for the rotorcraft. This allowed the flight duration in brownout to be linked to reductions in engine performance.

It is shown that NGV stage efficiency reduces with increasing surface roughness in a non-linear manner. Over the surface roughness range considered in this work, stage performance losses translate to linear changes in core mass flow rate, efficiency, turbine exit temperature and specific fuel consumption of the whole engine. It has been shown that changes in surface roughness of the high pressure turbine can result in efficiency reductions and turbine exit temperature increases of up to 1% compared to the 'clean' design point of the engine. The rate at which these parameters degrade has been shown to be a function of the brownout concentration of the particular rotorcraft

under consideration. The HH-60 is seen to experience more rapid engine degradation than the UH-1Y due to its increased brownout concentration. As a result, it is subject to a 1% efficiency drop after only 38 minutes of brownout flight whereas the UH-1Y can operate in excess of 120 minutes without exceeding this limit.

The results obtained here are under-predictions of the total damage and reduction in engine performance as they account only for changes in surface roughness. They do not account for additional losses due to the reduction in engine flow path areas caused by accumulation of molten particulate on NGVs. Additionally, the similarity between the GE-E<sup>3</sup> and T700 NGV geometries is unknown. The incorporation of the actual T700 NGV geometry into the model would greatly improve its validity. Finally, the work carried out here has assumed a uniform distribution of surface roughness along the NGV chord. This is suitable for a first-order approximation of performance loss. However, in future it would be ideal to spatially specify the local roughness variations. This will allow the elevated roughness due to biasing of deposits at leading and trailing edges of NGVs to be accounted for in the model.

This work is best viewed as a demonstration of a method by which changes in sub-system performance can be implemented into a wider, whole engine modelling approach. The method is demonstrated for particulate accretion damage on HPT NGV's and the changes in surface roughness this causes. It is however just as applicable for assessing damage in other engine components such as compressor damage or latter turbine stages.

## 6. FUTURE WORK

With the incorporation of methodology improvements such as the inclusion of NGV throat blockage effects, and localised surface roughness variations, the work presented in this contribution has multiple benefits to rotorcraft operators. It is envisioned that this methodology will aid operational decisions such as determining mission capability and maintenance scheduling. By combining dosages corresponding to safe and unsafe operations with known brownout concentrations, flight durations at which safety is compromised can be ascertained. At the most basic level, this can provide a go or no-go decision for a particular mission. In the longer term, it would allow the performance reduction expected from a campaign of missions to be determined along with the flight duration after which engines must be rejected. This would allow a shift towards prognostic scheduling of maintenance for the operator, reducing engine

rejection rates, platform downtime and unnecessary maintenance costs.

## 7. ACKNOWLEDGMENTS

The authors would like to pay special thanks, to the project sponsors; the Defence, Science and Technology Laboratory (DSTL) and EPSRC who have made this work possible. Additional thanks to the Vertical Lift Network, EPSRC EP/M018164/1 (VLN) for their support.

## 8. NOMENCLATURE

### ABBREVIATIONS

CFD	<i>Computational Fluid Dynamics</i>
EAPS	<i>Engine Air-Particle Separator</i>
EGT	<i>Exhaust Gas Temperature</i>
GSP	<i>Gas Turbine Simulation Program</i>
HPT	<i>High Pressure Turbine</i>
LPT	<i>Low Pressure Turbine</i>
NGV	<i>Nozzle Guide Vane</i>
OSU	<i>Ohio State University</i>
RMS	<i>Root Mean Squared</i>
SFC	<i>Specific Fuel Consumption</i>
SST	<i>Shear Stress Transport</i>
TBC	<i>Thermal Barrier Coating</i>
TET	<i>Turbine Exit Temperature</i>
YPG	<i>Yuma Proving Ground</i>

### GREEK SYMBOLS

$\delta$	<i>Dosage [mg.s/m<sup>3</sup>]</i>
$\eta$	<i>Efficiency [-]</i>
$\sigma$	<i>Particulate Concentration [mg/m<sup>3</sup>]</i>
$\nu$	<i>Kinematic Viscosity [m<sup>2</sup>/s]</i>
$\Delta$	<i>Change in a Variable [-]</i>
$\Lambda$	<i>Stage Reaction [-]</i>
$\Phi$	<i>Stage Flow Coefficient [-]</i>
$\psi$	<i>Stage Loading [-]</i>

### ROMAN SYMBOLS

$R$	<i>Surface Roughness [<math>\mu</math>m]</i>
$T$	<i>Temperature [K]</i>
$U$	<i>Linear Rotational Velocity [m/s]</i>
$V$	<i>Linear Velocity [m/s]</i>
$W$	<i>Mass Flow Rate [kg/s]</i>
$c_p$	<i>Specific Heat Capacity</i>
$k_s$	<i>Equivalent Sandgrain Roughness [<math>\mu</math>m]</i>
$t$	<i>Time [s]</i>

### SUPERSCRIPTS

[.]'	<i>Denotes Isentropic Conditions</i>
------	--------------------------------------

### SUBSCRIPTS

[.] <sub>a</sub>	<i>Surface Averaged Value</i>
[.] <sub>q</sub>	<i>Root Mean Squared Value</i>
[.] <sub>p</sub>	<i>Pertaining to the Particle</i>
[.] <sub>rel</sub>	<i>Relative Conditions</i>
[.] <sub>x</sub>	<i>Engine Axial Direction</i>
[.] <sub>N</sub>	<i>Pertaining to the Nozzle</i>
[.] <sub>0</sub>	<i>Total Conditions</i>
[.] <sub>1</sub>	<i>Stage Entry</i>
[.] <sub>2</sub>	<i>Nozzle Exit/Rotor Entry</i>
[.] <sub>3</sub>	<i>Stage Outlet</i>

## 9. REFERENCES

- [1] A. J. Wadcock, L. A. Ewing, and E. Solis, "Rotorcraft Downwash Flow Field Study to Understand the Aerodynamics of Helicopter Brownout," in *Technologies for the Next Generation of Vertical Lift Aircraft*, Dallas-Fort Worth, 2008, p. 27.
- [2] M. Dunn, "Operation of gas turbine engines in an environment contaminated with volcanic ash," *J. Turbomach.*, vol. 134, no. 5, p. 051001, 2012.
- [3] R. J. Clarkson, E. J. Majewicz, and P. Mack, "A re-evaluation of the 2010 quantitative understanding of the effects volcanic ash has on gas turbine engines," *Proc. Inst. Mech. Eng. Part G J. Aerosp. Eng.*, vol. 230, no. 12, pp. 2274–2291, Oct. 2016.
- [4] G. R. Whitehouse, D. A. Wachspress, and T. R. Quackenbush, "Aerodynamic Design of Helicopter Rotors for Reduced Brownout," presented at the International Powered Lift Conference, Philadelphia, 2010, p. 14.
- [5] O. Sweetman, "Hawaii V-22 Accident Investigation Points to New Ingestion Issue," *Aviation Week & Technology*, 2015. .
- [6] J. Milluzzo and J. Leishman, "Assessment of Rotorcraft Brownout Severity in Terms of Rotor Design Parameters," *J. Am. Helicopter Soc.*, vol. 55, no. 3, pp. 32009–320099, Jul. 2010.
- [7] C. Cowherd Jr, "Sandblaster 2 Support of See-Through Technologies for Particulate Brownout," Midwest Research Institute, 2007.
- [8] J. Savage, W. Harrington, R. A. McKinley, H. N. Burns, S. Braddom, and Z. Szoboszlai, "3D-LZ helicopter lidar imaging system," in *SPIE*, 2010, vol. 7684, p. 768407.
- [9] N. Bojdo and A. Filippone, "Comparative Study of Helicopter Engine Particle Separators," *J. Aircr.*, vol. 51, no. 3, pp. 1030–1042, May 2014.
- [10] M. G. Dunn, A. Baran, and J. Miatch, "Operation of gas turbine engines in volcanic ash clouds," in *ASME Journal of Engineering for Gas Turbines and Power*, The Hague, 1994, vol. 118, pp. 724–731.
- [11] R. J. Clarkson and H. Simpson, "Maximising Airspace Use during Volcanic Eruptions: Matching Engine Durability against Ash Cloud Occurrence," North Atlantic Treaty Organisation Science & Technology Organisation, MP-AVT-272-1, 2017.
- [12] J. Smialek, "The Chemistry of Saudi Arabian Sand: A Deposition Problem on Helicopter Turbine Airfoils," 1991.
- [13] M. B. Krisak, "Environmental Degradation of Nickel-Based Superalloys Due to Gypsiferous Desert Dusts," Air Force Institute of Technology, Wright Patterson Air Force Base, 2015.
- [14] R. P. Taylor, "Surface Roughness Measurements on Gas Turbine Blades," presented at the Gas Turbine and Aeroengine Congress and Exposition, Toronto, 1989, p. 7.
- [15] J. L. Boynton, R. Tabibzadeh, and S. T. Hudson, "Investigation of Rotor Blade Roughness Effects on Turbine Performance - Boynton et.al.pdf," presented at the 37th International Gas Turbine and Aeroengine Congress and Exposition, Cologne, 1993, vol. 115, pp. 614–620.
- [16] R. J. Boyle and R. G. Senyitko, "Measurements and Predictions of Surface Roughness Effects on Turbine Vane Aerodynamics," presented at the ASME Turbo Expo, Atlanta, 2003, p. 13.
- [17] H. Matsuda, F. Otomo, H. Kawagishi, A. Inomata, Y. Niizeki, and T. Sasaki, "Influence of Surface Roughness on Turbine Nozzle Profile Loss and Secondary Loss," 2006, vol. 2006, pp. 781–788.
- [18] F. Hummel, M. Lötzerich, P. Cardamone, and L. Fottner, "Surface Roughness Effects on Turbine Blade Aerodynamics," *J. Turbomach.*, vol. 127, no. 3, p. 453, 2005.
- [19] A. Kellersmann, S. Weiler, C. Bode, J. Friedrichs, G. Ramm, and J. Stading, "Surface Roughness Impact on Low-Pressure Turbine Performance due to Operational Deterioration," p. 10, 2017.
- [20] J. Jensen, S. Squire, J. Bons, and T. Fletcher, "Simulated land-based turbine deposits generated in an accelerated deposition facility," *J. Turbomach.*, vol. 127, no. 3, pp. 462–470, 2005.
- [21] J. E. Wammack, J. Crosby, D. Fletcher, J. P. Bons, and T. H. Fletcher, "Evolution of Surface Deposits on a High-Pressure Turbine Blade—Part I: Physical Characteristics," *J. Turbomach.*, vol. 130, no. 2, p. 021020, 2008.
- [22] J. P. Bons, "A Review of Surface Roughness Effects in Gas Turbines," *J. Turbomach.*, vol. 132, no. 2, p. 021004, 2010.
- [23] D. G. Bogard, D. L. Schmidt, and M. Tabitta, "Characterization and Laboratory Simulation of Turbine Airfoil Surface Roughness and Associated Heat Transfer," *J. Turbomach.*, vol. 120, pp. 337–342, 1998.
- [24] N. Bojdo and A. Filippone, "Effect of Desert Particulate Composition on Helicopter Engine Degradation Rate," presented at the European Rotorcraft Forum, Southampton, 2014.
- [25] H. Cohen, G. F. C. Rogers, and H. I. H. Saravanamuttoo, *Gas Turbine Theory*, 4th Edition. Harlow: Longman, 2009.
- [26] W. P. J. Visser and M. Broomhead, *GSP: A generic object-oriented gas turbine simulation environment*. National Aerospace Laboratory NLR, 2000.
- [27] G. A. Misté and E. Benini, "Performance of a Turboshaft Engine for Helicopter Applications Operating at Variable Shaft Speed," presented at the Gas Turbine India Conference, Mumbai, 2012, pp. 701–715.

---

### Copyright Statement

The authors confirm that they, and/or their company or organization, hold copyright on all of the original material included in this paper. The authors also confirm that they have obtained permission, from the copyright holder of any third party material included in this paper, to publish it as part of their paper. The authors confirm that they give permission, or have obtained permission from the copyright holder of this paper, for the publication and distribution of this paper as part of the ERF proceedings or as individual offprints from the proceedings and for inclusion in a freely accessible web-based repository.